Tunable reflectance spectra of multilayered cholesteric photonic structures with anisotropic defect layers

E. M. Nascimento, F. M. Zanetti, M. L. Lyra, and I. N. de Oliveira
Instituto de Física, Universidade Federal de Alagoas, Maceió, AL 57072-970, Brazil
(Received 15 October 2009; published 26 March 2010)

In this paper, we investigate the spectral characteristics of normal incident light reflected by a multilayered structure composed of an alternated sequence of single-pitch cholesteric liquid-crystal (ChLC) and anisotropic layers. Using the Berreman 4×4 matrix formalism, we numerically obtain the reflection spectrum and the chromaticity diagram as a function of the anisotropic layers thickness d. For $d\to0$, the structure behaves like a single ChLC layer, showing a single reflection band. As the anisotropic layer thickness increases, the reflection band shifts toward high-wavelength spectral regions, while new reflection bands appear. As a consequence, the reflection chromaticity continuously changes with d. It is observed that a suitable choice of the anisotropic layer thickness can produce a threefold reflection band with a red-green-blue associated color for both polarized and unpolarized incident lights.

DOI: 10.1103/PhysRevE.81.031713 PACS number(s): 42.70.Df, 42.70.Qs, 61.30.−v

I. INTRODUCTION

Optical properties of one-dimensional multilayered structures have attracted a considerable interest due to their relevance for the development of new electro-optical devices [1–5]. In particular, these systems exhibit a frequency range of reflected modes, denominated photonic band gap, which can be suitably tuned by modifying their internal stacked structure [6]. Such a behavior has been explored in the design of tunable filters [1], all-optical switches [2], and low-threshold lasers [4]. From a fundamental point of view, photonic systems present a rich phenomenology associated with interface effects [7,8], nonlinear response [9,10], and the introduction of disorder and defect layers [11,12]. In fact, emission of coherent thermal radiation [13], optical localization transitions [14], and propagation of spatial solitons [15] are a few examples of the wide scope of this subject in different research areas.

Over the past decade, several works have been devoted to the study of one-dimensional photonic structures containing cholesteric liquid-crystal (ChLC) layers [12,16–22]. Cholesteric liquid crystals consist of a chiral nematic sample, which is characterized by a periodic helical distortion of the nematic orientational order [23]. With a pitch comparable with the optical wavelength, such a self-organized structure behaves as a pseudophotonic system for circularly polarized light with the same handedness of the director distortion. This unique property has provided the possibility of designing tunable mirrorless laser devices that explore the pitch sensitivity to external agents, such as an electric field [23], temperature [24] and concentration [25] gradients, and uv irradiation [26–28]. The above feature has been explored to develop broadband reflectors based on cholesteric systems with a continuous pitch gradient [18,19,25,29,30]. Further, it was demonstrated that the introduction of defects in the helical structure induces the emergence of resonance modes inside the photonic stop band [12,16,31–33]. The generation and setting of these modes from different mechanisms have been extensively studied due to their high-wavelength selectivity, which is required by many electro-optical applications. Defect modes are usually associated with a discontinuous point in the helical periodicity (twist defect) [31] and with the inclusion of isotropic layers [12] or anisotropic layers (AnL's) [34] in the cholesteric structure (defect layer). In this case, the anisotropic layer corresponds to a slab with an optical axis without a helicoidal distortion, in contrast to the cholesteric layers. Actually, recent investigations reported that the inclusion of a single anisotropic defect layer provides an additional degree of freedom for tuning the defects modes, with a weaker polarization dependence [34–36].

The selective reflection of stacked structures containing cholesteric liquid-crystal layers has attracted a renewed interest. In particular, these systems exhibit a complex reflection spectrum which can be described as a multiple photonic band-gap structure [20]. Such a behavior contrasts with the typical single-band reflection of cholesteric liquid crystals presenting a defect layer or a twist defect [12,31]. In fact, numerical and experimental studies have revealed that the multiband reflection spectrum depends on the internal arrangement of the system [20,37,38]. Introducing quasiperiodic Fibonnacian twist defects in a single-pitched cholesteric structure, recent works have demonstrated that a red-green-blue (RGB) reflection spectrum takes place when a $\pi/3$ phase jump is inserted in the helical periodicity [37]. Depending on the Fibonnacian generation, such a RGB reflection spectrum was predicted to persist in a wide range of incidence angles [38]. Similar results were also obtained in multilayered structures consisting of an alternated sequence of single-pitched cholesteric layers and isotropic dielectric slabs under normal incidence. However, it was observed that the reflection spectrum and chromaticity diagram of alternated sequences exhibit a pronounced dependence on the incidence angle [38], presenting a complex sequence of color shifts. Although the reflection properties of cholesteric multilayered structures containing twist defects and isotropic defect layers have been extensively investigated, the effects associated with the introduction of multiple anisotropic defect layers have not been explored so far.

In this work, we investigate the reflection properties of multilayered structures constituted by alternated cholesteric

and anisotropic layers, considering the normal incidence of circularly polarized optical waves with positive and negative handedness of the director distortion. By using the Berreman 4×4 matrix formalism [39,40], we observe that the multiband reflection spectrum of the system can suitably be adjusted by setting the thickness of the anisotropic layer. According the International Commission on Illumination prescription (CIE 1931) [41], the chromaticity diagram of this structure is also computed, with RGB reflection bands being observed for a typical set of experimental parameters, thus leading a white chromaticity of the reflected light. Further, our results show that the introduction of the anisotropic defect layer reduces the reflection dependence on the polarization handedness of the optical wave.

II. BERREMAN 4×4 MATRIX FORMALISM

In order to study the reflection properties of multilayered structures containing cholesteric liquid-crystal layers, we used the Berreman 4×4 numerical method which permits us to investigate the light propagation in a medium with a nonuniform refractive index along one direction. In particular, we considered a monochromatic plane wave of angular frequency ω, circularly polarized, and propagating in a medium that is uniform in its dielectric properties in one plane, which is taken to be the xy plane. The x-y components of the electric field E and the magnetic field H can be written as

$$\begin{pmatrix} E_x(\vec{r},t) \\ E_y(\vec{r},t) \\ H_x(\vec{r},t) \\ H_y(\vec{r},t) \end{pmatrix} = \psi(z)e^{-i\omega t}, \tag{1}$$

where $\psi(z)$ is a column vector and normal incidence was assumed. From the Maxwell's equations in Gaussian units, one can derive the following set of four differential equations:

$$\frac{d\psi(z)}{dz} = ikD(z)\cdot\psi(z), \tag{2}$$

where D is the so-called Berreman 4×4 matrix [39,40]. Assuming the medium to be nonmagnetic with a constant dielectric tensor ε, the Berreman matrix does not depend on z and can be written as

$$D = \begin{pmatrix} 0 & 0 & 0 & 1 \\ 0 & 0 & -1 & 0 \\ \varepsilon_{yz}\dfrac{\varepsilon_{zx}}{\varepsilon_{zz}} - \varepsilon_{yx} & -\varepsilon_{yy} + \varepsilon_{yz}\dfrac{\varepsilon_{zy}}{\varepsilon_{zz}} & 0 & 0 \\ \varepsilon_{xx} - \varepsilon_{xz}\dfrac{\varepsilon_{zx}}{\varepsilon_{zz}} & \varepsilon_{xy} - \varepsilon_{xz}\dfrac{\varepsilon_{zy}}{\varepsilon_{zz}} & 0 & 0 \end{pmatrix}. \tag{3}$$

Several numerical methods have been successfully employed to solve the Berreman equation, presenting good agreement with the experimental results [12,18,39]. Here, we express the solution of Eq. (2) as a superposition of four distinct plane waves,

$$\psi(z) = \sum_{l=1}^{4} C_l\psi^{(l)}e^{ik\lambda_l z}, \tag{4}$$

where $\psi^{(l)}$ are the eigenvectors and λ_l are the eigenvalues of the Berreman matrix. For a ChLC layer of thickness a, the helical distortion of the director implies a z dependence of the Berreman matrix, which invalidates the above exact solution. However, an approximate numerical solution can be obtained by virtually slicing the cholesteric layer into a large number M of thin slabs. In this case, D can be treated as fairly constant within each slab. The relation between the electric and magnetic fields at the interfaces at $z=z_1$ and $z=z_1+a$ can be written in transfer matrix form as

$$\psi(z_1+a) = \mathcal{T}_1\cdot\mathcal{T}_2\cdot\cdots\cdot\mathcal{T}_M\cdot\psi(z_1), \tag{5}$$

$$\mathcal{T}_i = \Psi_i\Gamma_i\Psi_i^{-1}, \tag{6}$$

where $\mathcal{T}_i$ is the transfer matrix associated with the ith virtual slice of the ChLC layer. Here, Ψ_i is a 4×4 unitary matrix whose columns are formed by the eigenvectors of D and Γ_i is a diagonal matrix with elements $\Gamma_{l,l}=e^{ik\lambda_l\Delta z}$ $(\Delta z=\frac{a}{M})$.

In a multilayered structure, the boundary conditions require the parallel components of the electric and magnetic fields to be continuous at the interfaces. Therefore, the relation between the in-plane components of the fields at the two external interfaces which separate the film from the surrounding medium can be written as a function of the product of all transfer matrices, with no virtual slicing being needed for uniform and anisotropic layers.

The transfer matrix can be used to compute the transmittance and reflectance of the multilayered structure. For a normal incident plane wave, the components of the reflected (R_x,R_y) and transmitted (T_x,T_y) electric fields can be obtained from the following set of linear equations [40]:

$$\begin{aligned} E_x^i + R_x &= (F_{11}+F_{12}n_0)T_x + (F_{13}+F_{14}n_0)T_y, \\ n_0(E_x^i - R_x) &= (F_{21}+F_{22}n_0)T_x + (F_{23}+F_{24}n_0)T_y, \\ E_y^i + R_y &= (F_{31}+F_{32}n_0)T_x + (F_{33}+F_{34}n_0)T_y, \\ n_0(E_y^i - R_y) &= (F_{41}+F_{42}n_0)T_x + (F_{43}+F_{44}n_0)T_y, \end{aligned} \tag{7}$$

where E_x^i and E_y^i represent the components of the incident electric field and F_{ij}'s are the elements of the inverse transfer matrix $(F=\mathcal{T}^{-1})$. n_0 is the refractive index of the input medium, which we take as the typical value of glass cells $(n_0=1.5)$.

The multilayered structures incorporating ChLC layers were assumed to have the z direction as the twist axis. In these layers, the liquid-crystal director is represented by $\hat{n}=[\cos(q_0z),\sin(q_0z),0]$, where $q_0=2\pi/P$, and P is the helical pitch. For the anisotropic layer, the optical axis is constant and its orientation coincides with the nematic director at the cholesteric layer interfaces. In such a configuration, no twist defect is generated by the introduction of anisotropic layer in the helical structure. In all cases, the dielectric tensor function $\varepsilon(z)$ is given by $\varepsilon_{i,j}=\varepsilon_\perp\delta_{i,j}+\Delta\varepsilon n_i n_j$. Here, $(i,j)\in x,y,z$, $\delta_{i,j}$ is the Kronecker delta, and $\Delta\varepsilon=(\varepsilon_\parallel-\varepsilon_\perp)$ [23].

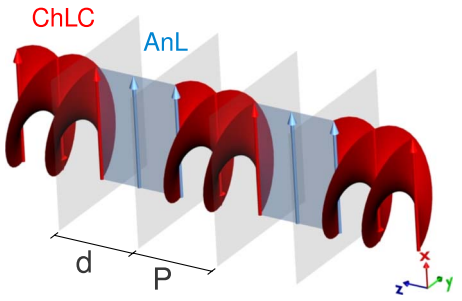

FIG. 1. (Color online) Scheme of the multilayered structure composed of an alternate sequence of cholesteric liquid-crystal (ChLC) layers and AnL's. The anisotropic director vector orientation matches the ChLC layer director orientation at the interfaces (no twist defect).

III. RESULTS

We analyzed the spectral properties of a multilayered structure composed of an alternated sequence of cholesteric and anisotropic layers, as presented in Fig. 1. The ordinary and extraordinary refractive indices of the birefringent planes were taken to be $n_o^a=1.342$ ($\varepsilon_\perp=n_o^2=1.8$) and $n_e^a=1.449$ ($\varepsilon_\parallel=n_e^2=2.1$) for the anisotropic layers, in order to allow a closer connection with previous theoretical studies of cholesteric structures with a single anisotropic defect layer [34]. The case of isotropic defect layers with a refraction index $n=(n_e^a+n_o^a)/2$ was computed for comparison. For the cholesteric layers, we used $n_o=1.56$ and $n_e=1.78$, which are typical values for polymeric cholesteric liquid crystal [21]. The optical pitch is given by $\lambda_P=\bar{n}P=532$ nm, where $\bar{n}$ is the average refractive index given by $\bar{n}=[(n_o^2+n_e^2)/2]^{1/2}$, in such a way that the main reflection band of cholesteric system is centered in the green region of the optical spectrum, as used in previous theoretical and experimental studies [20,37]. Imposing the outermost layers to be cholesteric liquid crystals, the lowest-order alternated sequences are defined as $S_1=A$, $S_2=ABA$, $S_3=ABABA$, and $S_4=ABABABA$. A and B represent the ChLC and anisotropic layers, respectively. In alternated sequences, enhancing the number of layers leads to a multifragmented spectrum and a high reflectance around the main band gap. In what follows, we will investigate the reflection properties of the S_4 alternated sequence, which is able to display a nearly RGB spectrum with a relatively high reflectance [38].

In Fig. 2 we present the density plot of the reflection spectrum as a function of the thickness of the defect layers d for the cases of isotropic and anisotropic defects. Here, we consider a normal incident light presenting a circular polarization with the same handedness of the cholesteric helix. The brighter areas represent the reflection peaks for a given optical wavelength and defect layer thickness. For $d\to 0$, the multilayered structure is reduced to a single ChLC layer with a total thickness of $4P$, presenting a single reflection band. A different scenario is observed when the defect layer thickness becomes comparable to the helical pitch, with the appearance of new reflection bands. Further, we notice that the original stop band is shifted toward longer-wavelength regions. In fact, the number and position of the reflection bands can be

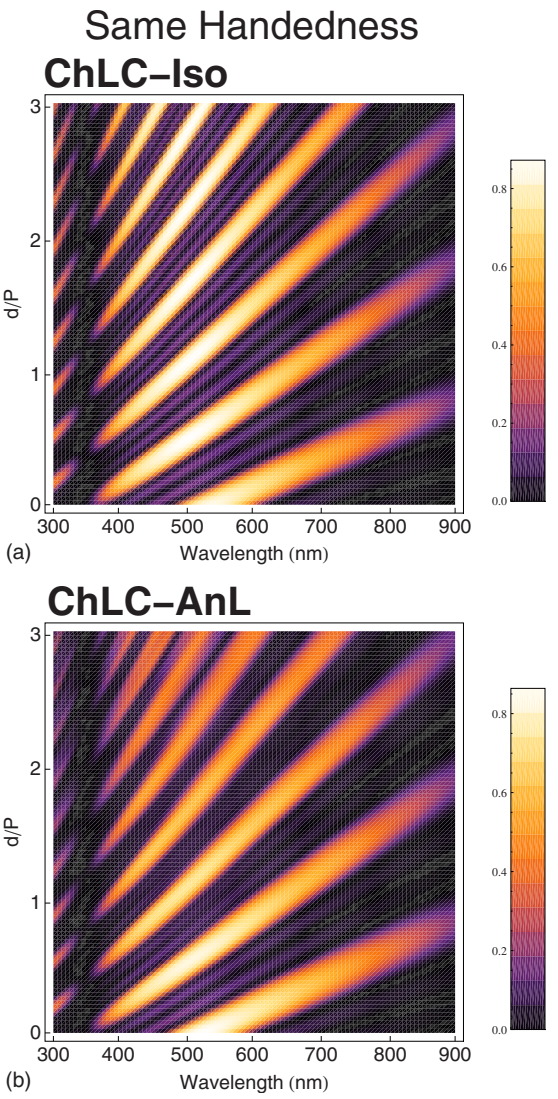

FIG. 2. (Color online) Density plot of the reflection spectra as a function of the defect layer thickness d, in units of the helical pitch P for the S_4 structure and normal incident light with the circular polarity handedness coinciding with the helical distortion of the ChCL director. (a) Isotropic and (b) anisotropic defects. The brighter areas represent the maxima of reflection. Notice that the reflection peaks are shifted toward the region of longer wavelengths as the defect layer thickness increases. The structure with anisotropic defects exhibits a lower reflectance peaks due to the phase retardation effect.

controlled by adjusting the thickness of the defect layers. In the limit of $d\gg P$, the reflection spectrum shows a large number of stop bands with similar peak amplitudes. The structure with anisotropic defects exhibits lower reflectance peaks due to the phase retardation effect. Such a feature is more pronounced for large thicknesses of the anisotropic layers.

The chromatic sensation of human eyes to a specific optical spectrum is usually characterized by a chromaticity diagram. In what follows, we use the CIE 1931 prescription which is based on the *tristimulus* values of a color, representing the intensity combination of primary colors basis. The numerical representation of the tristimulus for the CIE XYZ color space is given by [41]

$$X = \int_0^\infty I(\lambda)\bar{x}(\lambda)d\lambda,$$

$$Y = \int_0^\infty I(\lambda)\bar{y}(\lambda)d\lambda,$$

$$Z = \int_0^\infty I(\lambda)\bar{z}(\lambda)d\lambda, \tag{8}$$

where $I(\lambda)$ is the optical spectrum and $\bar{x}$, $\bar{y}$, and $\bar{z}$ are the *color matching functions* obtained experimentally for a CIE standard observer. The chromaticity is represented on the diagram by a point of coordinates (x,y) defined as

$$x = \frac{X}{X+Y+Z},$$

$$y = \frac{Y}{X+Y+Z}, \tag{9}$$

with $x=y=1/3$ corresponding to the white chromaticity.

The reflection chromaticity of multilayered structures is directly associated with the multiple stop bands in the reflection spectrum [38]. In particular, the chromaticity diagram of the S_4 alternated sequence exhibits a pronounced color shift as the defect layer thickness is changed for both isotropic and anisotropic defects, as shown in Fig. 3. Here, the circular polarization of the normal incident light still presents the same handedness of the cholesteric helix. In the limit of $d \to 0$, the single ChLC layer presents only one associated color reflection band located on the green region. However, such a band is shifted toward the red region as the defect layer thickness increases. Further, a complex sequence of color shifts is observed as other stop bands emerge in the visible range of the spectrum. For thick defect layers, the reflection spectrum presents several stop bands, which results in an associated chromaticity around the white region. Although the chromaticities are similar for thin isotropic and anisotropic defect layers, the chromaticity of the structure containing anisotropic defect layers becomes more concentrated around the white region for thick layers.

The introduction of isotropic defect layers in a cholesteric system gives rise to multiple band gaps when the light polarization matches the helical distortion sign, as shown in Fig. 2. For the incident light polarization and cholesteric helix with opposite handedness, the reflection spectrum of the multilayered structure with isotropic defects [Fig. 4(a)] exhibits a behavior similar to that of an alternated sequence containing only isotropic dielectric layers. Replacing the isotropic defects in the multilayered arrangement with anisotropic layers, a distinct behavior can be observed in the photonic properties of the system, as shown in Fig. 4(b). Here, we present the density plot of the reflection spectrum as a function of the thickness d of the defect layers for the incident light polarization and cholesteric helix with opposite handedness. For the S_4 alternated sequence containing thin anisotropic layers ($d<P$), we notice that the band-gap pattern (brighter areas) is quite similar to that of the structure

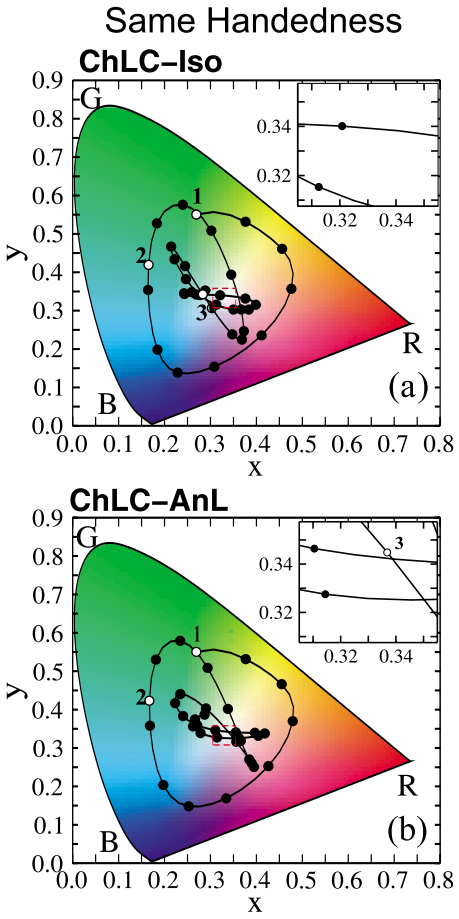

FIG. 3. (Color online) CIE 1931 chromaticity diagram of the S_4 alternated sequence of cholesteric and defect layers: (a) Isotropic and (b) anisotropic defects. The normal incident light presents a circular polarity handedness coinciding with the helical distortion of the ChCL director. The continuous line represents a guide to the eyes for the trajectory of the reflected light chromaticity as the thickness of the defect layer is varied from $d=0$ to $d=2P$ in $0.06P$ steps (filled circles). The open circles correspond to (1) $d=0$, (2) $d=0.5P$, and (3) $d=1.04P$. The inset shows a magnification near the white region ($x=y=0.33$).

with isotropic defect layers. On the other hand, a multiple band-gap structure emerges as the anisotropic layer thickness increases, a feature not observed in the case of isotropic defects. In fact, a large number of stop bands are observed in the limit of $d \gg P$, with the band peaks presenting almost identical amplitudes. This behavior is directly associated with the reduction in the polarization sensitivity of the optical properties of multilayered systems.

The emergence of a multiple photonic band gap with the enhancement of the anisotropic layer thickness is presented in Fig. 5, considering the incident light with different polarizations. We also show the blue, green, and red color matching functions used to compute the chromaticity diagram. For an incident light polarization with the same handedness of the cholesteric helix (solid line), we notice that an approximate white chromaticity is obtained for $d=1.04P$ (see Fig. 3). In addition, we observe a significant reduction in the reflectance, although the number of stop bands increases for

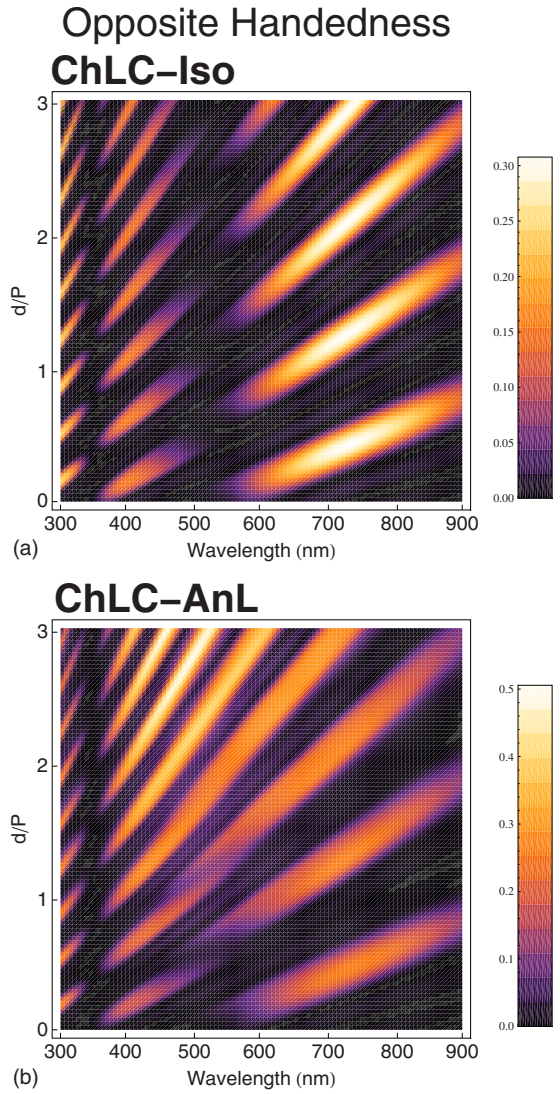

FIG. 4. (Color online) Density plot of the reflection spectra as a function of defect layer thickness d, in units of the helical pitch P, for circularly polarized light with handedness opposite to the ChLC director helix: (a) Isotropic and (b) anisotropic defects. Notice that the reflection peaks in the presence of anisotropic defects become higher (brighter) as d increases reflecting the fact that the reflectance becomes insensitive to the light polarization.

$d=2.5P$. This behavior contrasts to that of typical photonic band-gap materials which present an enhancement in the reflectance with the sample thickness. On the other hand, the reflectance increases with the thickness of the anisotropic layer for an incident light polarization with the opposite handedness of the cholesteric helix (dashed line). Therefore, the reflection spectrum presents a band-gap pattern with a weak dependence on the optical polarization when the anisotropic layers become thicker than the helical pitch. It is important to stress that all results were obtained for a fixed optical pitch λ_P. In this case, the multilayered structure develops reflection bands close to the RGB color matching functions. By varying λ_P for a fixed defect layer thickness d, the reflection bands shift, resulting in different chromaticities of the reflected light.

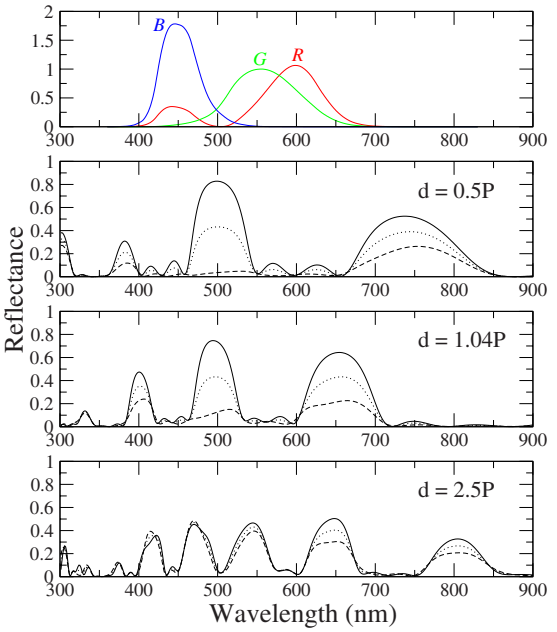

FIG. 5. (Color online) Reflection spectrum of the S_4 alternated sequence with anisotropic defects for the incident light presenting distinct polarization states: same handedness of ChLC (solid line), opposite handedness of ChLC (dashed line), and unpolarized (dotted line). The color matching functions used to obtain the chromaticity diagrams are also exhibited in the top panel, labeled R (red), G (green), and B (blue). As the anisotropic layer thickness increases, a multiple band-gap structure emerges which weakly depends on the incident light polarization.

The above results demonstrate that the introduction of anisotropic layers affects significantly the optical properties of multilayered systems containing cholesteric liquid crystals. In particular, the anisotropic layers promote a reduction in the polarization sensitivity of the reflection spectrum, with a simultaneous decrease in the stop band peaks. In fact, each anisotropic layer behaves as a phase retarder which modifies the polarization of the light propagating through it. More specifically, the rotation of the light polarization takes place due to the continuous variation in the relative phase between the two optical eigenmodes in a birefringent medium. Such an effect has been recently explored in the design of tunable-electroluminescent devices and low-threshold lasers constituted by a cholesteric liquid crystal containing a single anisotropic defect [34–36]. However, long alternated sequences present a rich phenomenology associated with multiple phase retardation which can be reasonably employed in optical devices based on their reflection properties, such as optical switches and reflective color displays without the use of a back light.

The rich phenomenology associated with multiple phase retardation in S_4 alternated sequences can be illustrated by their reflection chromaticity for different light polarizations, as shown in Fig. 6. For a light polarization with a handedness opposite to the cholesteric helix, we notice that the chromaticity presents a sequence of color shifts as the anisotropic layer thickness increases [Fig. 6(b)], which occurs in a more restricted region than that observed in Fig. 3. In particular, we observe that the chromaticity describes a trajectory

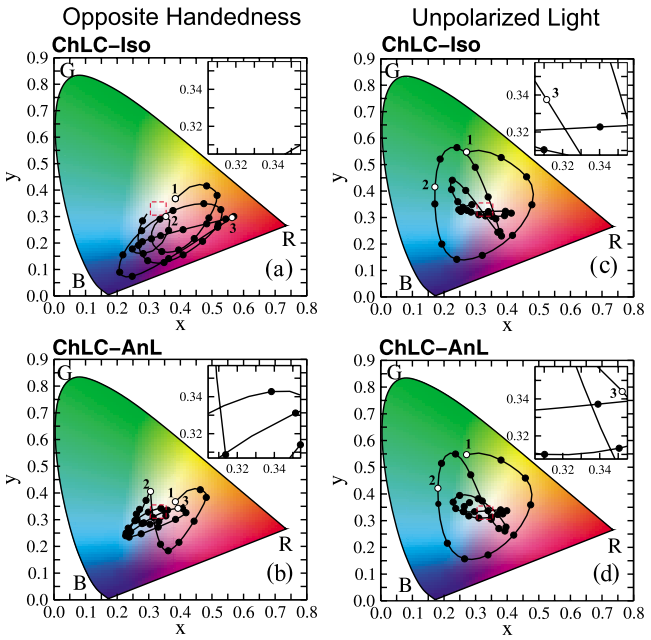

FIG. 6. (Color online) CIE 1931 chromaticity diagram of S_4 alternated sequences of cholesteric and defects layers: (a) isotropic and (b) anisotropic defects for an incident light with a polarization state opposite to the cholesteric helix. The thickness step and symbols are the same as in Fig. 3. For the anisotropic defects, we notice that a complex sequence of color shifts takes place in a more restrict region of the spectrum. For unpolarized incident light, S_4 alternated sequences containing (c) isotropic and (d) anisotropic defects present similar reflection chromaticity diagrams. The inset shows a magnification near the white region ($x=y=0.33$).

around the white region, which reflects the emergence of multiple band gaps in the reflection spectrum as d is enhanced. Such a behavior contrasts to that observed in the S_4 structure containing isotropic defects [Fig. 6(a)] for which the color shifts are more pronounced and displaced from the white region. For an unpolarized incident light, the reflection chromaticity of the structure with anisotropic defects [Fig. 6(d)] exhibits a similar sequence of color shifts as observed in Fig. 3 for $d<P$. In this case, the main contribution to the chromaticity comes from the matching of circular polarization and cholesteric helix. On the order hand, the contribution from the reverse of circular polarization and cholesteric helix becomes relevant as the anisotropic layer thickness becomes larger than the helical pitch. Consequently, the reflection chromaticity presents a distinct sequence of color shifts in comparison to the one displayed in Fig. 3. The above results open the possibility of designing reflective color displays from multilayered systems containing anisotropic and cholesteric layers. The reflection chromaticity diagram for the case of unpolarized incident light on a S_4 structure with isotropic defects is shown in Fig. 6(c) for completeness. Although it is similar to the one obtained for anisotropic defects, it results from quite distinct reflection spectra of the two light polarization components.

IV. CONCLUSION

In conclusion, we studied a structure composed of a cholesteric medium with the insertion of anisotropic defect layers, and analyzed the behavior of the reflection spectrum and its associated reflection chromaticity diagram as the thickness of defect layers is changed. For normal incident light (polarized with the same and opposite handiness of the ChLC, as well as unpolarized), it was observed a shift of the reflectance bands to high-wavelength regions and the creation of new bands as the thickness of the anisotropic layer d increases. This feature can make the variation of d a good parameter to shape the reflection spectrum in such a way to obtain a threefold RGB reflection chromaticity. We confirmed this possibility by plotting the CIE chromaticity diagrams where, for intermediate values of d, a reflection chromaticity near the white region was obtained. It is worthy to mention that in the fabrication of reflection displays it is quite valuable to obtain reflective structures and filters whose optical properties do not depend on the incident light polarization. Recently, it was experimentally demonstrated that the introduction of photopolymerizable monomers into a cholesteric medium can generate regions with helicity inversion after uv light curing [42,43]. Such a polymer-cholesteric gel behaves as an infrared hyper-reflective network that is almost independent on the light polarization. Our results indicate that the insertion of anisotropic defect layers in the ChLC matrices can be a good candidate to appease this need in the visible range. It is also interesting to stress that anisotropic media can still furnish other parameters, such as the director orientation and dielectric anisotropy, which can further contribute to the fine tuning of spectral characteristics of this class of systems, thus opening the possibility to tailor new multistructured optical devices.

ACKNOWLEDGMENTS

This work was partially supported by PRODOC-CAPES, INCT-FCx CNPq/MCT, and FINEP (Brazilian Research Agencies) as well as FAPEAL (Alagoas State Research Agency).

[1] K. L. Jim, D. Y. Wang, C. W. Leung, C. L. Choy, and H. L. W. Chan, J. Appl. Phys. **103**, 083107 (2008).
[2] A. E. Miroshnichenko, E. Brasselet, and Y. S. Kivshar, Appl. Phys. Lett. **92**, 253306 (2008).
[3] H. Taniyama, J. Appl. Phys. **91**, 3511 (2002).
[4] M. Loncar, T. Yoshie, A. Scherer, P. Gogna, and Y. M. Qiu, Appl. Phys. Lett. **81**, 2680 (2002).
[5] T. T. Larsen, A. Bjarklev, D. S. Hermann, and J. Broeng, Opt. Express **11**, 2589 (2003).
[6] J. D. Joannopoulos, R. D. Meade, and J. N. Winn, *Photonic Crystals: Modeling the Flow of Light* (Princeton University Press, Princeton, NJ, 1995).

[7] A. Chutinan and S. John, Phys. Rev. A **78**, 023825 (2008).
[8] A. P. Vinogradov, A. V. Dorofeenko, S. G. Erokhin, M. Inoue, A. A. Lisyansky, A. M. Merzlikin, and A. B. Granovsky, Phys. Rev. B **74**, 045128 (2006).
[9] V. Berger, Phys. Rev. Lett. **81**, 4136 (1998).
[10] S. F. Mingaleev and Y. S. Kivshar, Phys. Rev. Lett. **86**, 5474 (2001).
[11] Y. Lahini, A. Avidan, F. Pozzi, M. Sorel, R. Morandotti, D. N. Christodoulides, and Y. Silberberg, Phys. Rev. Lett. **100**, 013906 (2008).
[12] Y. C. Yang, C. S. Kee, J. E. Kim, H. Y. Park, J. C. Lee, and Y. J. Chon, Phys. Rev. E **60**, 6852 (1999).
[13] B. J. Lee, C. J. Fu, and Z. M. Zhang, Appl. Phys. Lett. **87**, 071904 (2005).
[14] Y. Lahini, R. Pugatch, F. Pozzi, M. Sorel, R. Morandotti, N. Davidson, and Y. Silberberg, Phys. Rev. Lett. **103**, 013901 (2009).
[15] A. A. Sukhorukov and Y. S. Kivshar, Phys. Rev. E **65**, 036609 (2002).
[16] R. Ozaki, Y. Matsuhisa, H. Yoshida, K. Yoshino, and M. Ozaki, J. Appl. Phys. **100**, 023102 (2006).
[17] T. Matsui, M. Ozaki, and K. Yoshino, Phys. Rev. E **69**, 061715 (2004).
[18] J. Y. Chen and L. W. Chen, J. Phys. D **38**, 1118 (2005).
[19] J. Y. Chen and L. W. Chen, Phys. Rev. E **71**, 061708 (2005).
[20] N. Y. Ha, Y. Takanishi, K. Ishikawa, and H. Takezoe, Opt. Express **15**, 1024 (2007).
[21] M. H. Song, N. Y. Ha, K. Amemiya, B. Park, Y. Takanishi, K. Ishikawa, J. W. Wu, S. Nishimura, T. Toyooka, and H. Takezoe, Adv. Mater. **18**, 193 (2006).
[22] B. Park, M. Kim, S. W. Kim, and I. T. Kim, Opt. Express **17**, 12323 (2009).
[23] P. G. De Gennes and J. Prost, *The Physics of Liquid Crystals* (Clarendon, Oxford, 1993).
[24] Y. Huang, Y. Zhou, and S. T. Wu, Appl. Phys. Lett. **88**, 011107 (2006).
[25] D. C. Zografopoulos, E. E. Kriezis, M. Mitov, and C. Binet, Phys. Rev. E **73**, 061701 (2006).
[26] S. Furumi, S. Yokoyama, A. Otomo, and S. Mashiko, Appl. Phys. Lett. **84**, 2491 (2004).
[27] S. Relaix, C. Bourgerette, and M. Mitov, Appl. Phys. Lett. **89**, 251907 (2006).
[28] S. Relaix, C. Bourgerette, and M. Mitov, Liq. Cryst. **34**, 1009 (2007).
[29] D. J. Broer, J. Lub, and G. N. Mol, Nature (London) **378**, 467 (1995).
[30] M. Belalia, M. Mitov, C. Bourgerette, A. Krallafa, M. Belhakem, and D. Bormann, Phys. Rev. E **74**, 051704 (2006).
[31] V. I. Kopp and A. Z. Genack, Phys. Rev. Lett. **89**, 033901 (2002).
[32] H. Yoshida, C. H. Lee, Y. Miura, A. Fujii, and M. Ozaki, Appl. Phys. Lett. **90**, 071107 (2007).
[33] J. Schmidtke, W. Stille, and H. Finkelmann, Phys. Rev. Lett. **90**, 083902 (2003).
[34] A. H. Gevorgyan and M. Z. Harutyunyan, Phys. Rev. E **76**, 031701 (2007).
[35] S. M. Jeong, N. Y. Ha, H. Takezoe, S. Nishimura, and G. Suzaki, J. Appl. Phys. **103**, 113101 (2008).
[36] M. H. Song, B. Park, K. C. Shin, T. Ohta, Y. Tsunoda, H. Hoshi, Y. Takanishi, K. Ishikawa, J. Watanabe, S. Nishimura, T. Toyooka, Z. Zhu, T. M. Swager, and H. Takezoe, Adv. Mater. **16**, 779 (2004).
[37] N. Y. Ha, Y. Ohtsuka, S. M. Jeonh, S. Nishimura, G. Suzaki, Y. Takanishi, K. Ishikawa, and H. Takezoe, Nature Mater. **7**, 43 (2008).
[38] E. M. Nascimento, I. N. de Oliveira, and M. L. Lyra, J. Appl. Phys. **104**, 103511 (2008).
[39] S. Stallinga, J. Appl. Phys. **85**, 3023 (1999).
[40] D. W. Berreman, J. Opt. Soc. Am. **62**, 502 (1972).
[41] H. R. Kang, *Computational Color Technology* (SPIE Press, Washington, D.C., 1993).
[42] M. Mitov and N. Dessaud, Nature Mater. **5**, 361 (2006).
[43] M. Mitov and N. Dessaud, Liq. Cryst. **34**, 183 (2007).